2026 International Nuclear Atlantic Conference – INAC 2026
Escola de Guerra Naval, Rio de Janeiro, RJ, August 24 - 28, 2026

Thermoluminescence and EPR Characterization of Cowrie Shell Powder for High-Dose Dosimetry Applications

B. F. Oliveira[1], D. N. Souza[2], and O. Rodrigues Jr.[1]

[1] *brunno.f@ipen.br, rodrijr@ipen.br, Nuclear and Energy Research Institute, 05508-000, São Paulo, SP, Brazil*

[2] *divanizia@gmail.com, Federal University of Sergipe, 49107-230, São Cristóvão, SE, Brazil*

1. Introduction

Cowrie shells are naturally occurring biomaterials widely found in nature and commonly used in jewelry and decorative artifacts [1,2,3]. Composed primarily of calcium carbonate ($CaCO_3$), these materials have attracted interest in radiation dosimetry, as they exhibit luminescent properties when exposed to high doses of ionizing radiation [4], enabling the quantification of absorbed dose through techniques such as thermoluminescence (TL). EPR spectroscopy has been employed in the dosimetric characterization of biomasses, due to its ability to identify and quantify radiation-induced paramagnetic centers. In these materials, irradiation promotes the formation of stable radicals, such as CO_2^- and CO_3^-, whose EPR signals exhibit intensity proportional to the absorbed dose [5,6,7,8,9].
In this context, the present study aims to characterize the dosimetric responses of cowrie shell samples of the species Cypraea tigris (T), Cypraea annulus (A), and Cypraea moneta (M), through Thermoluminescence (TL) and Electron Paramagnetic Resonance (EPR) techniques, evaluating the stability of the detected signals and the potential of this natural biomaterial as an alternative material for high-dose radiation dosimetry applications.

2. Methodology

The cowrie shells samples were broken, dried, and ground using a ceramic mortar and pestle, and the resulting powder was sieved to 75 μm and calcined at 300 °C. The powders were then weighed on an analytical balance and mixed with PTFE (Teflon) in a 1:1 mass ratio. The mixture was cooled to −5 °C for 1 h and pressed at 0.5 ton for 1 min, producing pellets. The pellets were sintered in a furnace at 400 °C for 1 h, followed by rapid cooling to room temperature. TL measurements were performed were performed using a Risø TL/OSL DA-20 reader with a heating rate of 5 °C/s up to 400 °C, using a Hoya U-340 optical filter (260–400 nm) and a Schott BG39 filter (400–600 nm). A 0.05 cm diameter collimator was employed to prevent signal saturation at high doses. EPR measurements were performed at room temperature using a Bruker EMXPlus, operating in the X-band.
For EPR measurements, the powder samples were weighed and placed in quartz tubes. The main EPR parameters are presented in Table I.

Table I: EPR parameters.

Parameter	Value	Parameter	Value
Microwave Frequency	9.847 GHz	Microwave Power	1.002 mW (23.0 dB attenuation)
Center Field	3500.0 G	Sweep Width	1000.0 G
Modulation Amplitude	1.000 G	Modulation Frequency	100.00 kHz
Gain	30 dB	Conversion Time	5.00 ms
Time Constant	0.01 ms	Sweep Time	50.00 s
Number of Scans	10	Resolution	10,000 points

3. Results and Discussion

3.1 TL emission curves with Schott BG39 filter.

Figure 1 presents the TL emission curves obtained from pellets of samples T, A, and M irradiated at 5 kGy, using the Schott BG39 filter, which exhibits transmittance in visible region. Upon examination of the emission curves, it can be observed that the TL emission of all samples displays well-defined peaks, with the principal emission occurring between 160–190 °C and a third peak at approximately 370 °C, with sample A exhibiting the highest luminescent intensity. This behavior may suggest the presence of multiple emission centers with distinct trap depths and different recombination mechanisms.

.

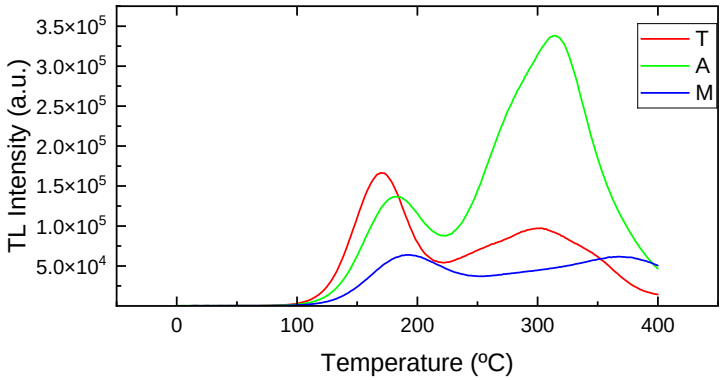
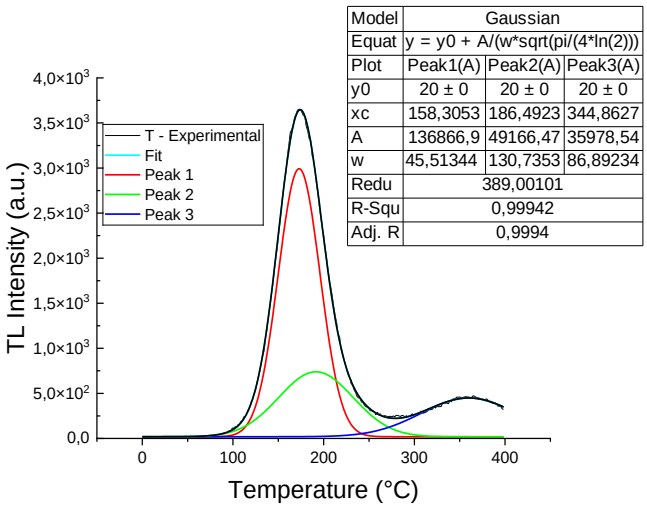


Figure 1: TL emission curves of samples T, A and M irradiated with 5 kGy (gamma radiation) using the Schott BG39 filter.

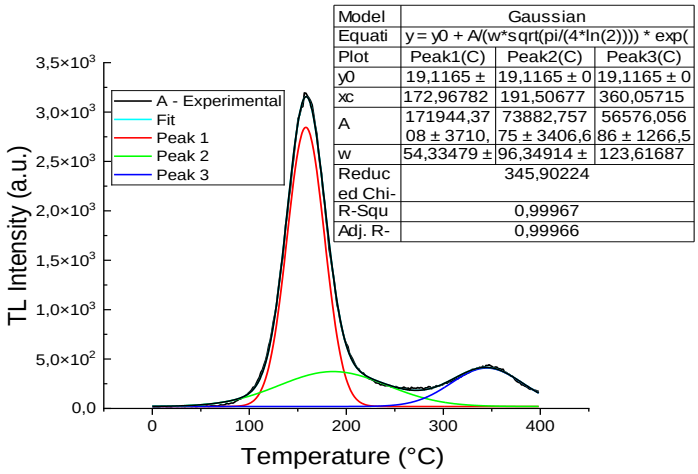
3.2 Deconvolution of the TL emission curves.

Figure 2, 3 and 4 presents the deconvolution of the TL emission curves of samples T, A, and M irradiated with 5 kGy (gamma radiation) using the Hoya UV-transmittance filter. All samples exhibited three peaks: the first corresponding to less thermally stable trapping centers, the second to more stable centers, and the third, of lower intensity, to deep traps requiring greater thermal stimulation. Peak temperatures and goodness-of-fit coefficients were as follows: sample T at ~173, 191, and 360 °C (R^2 = 0.99967); sample A at ~158, 186, and 345 °C (R^2 = 0.99942); and sample M at ~170, 250, and 366 °C.



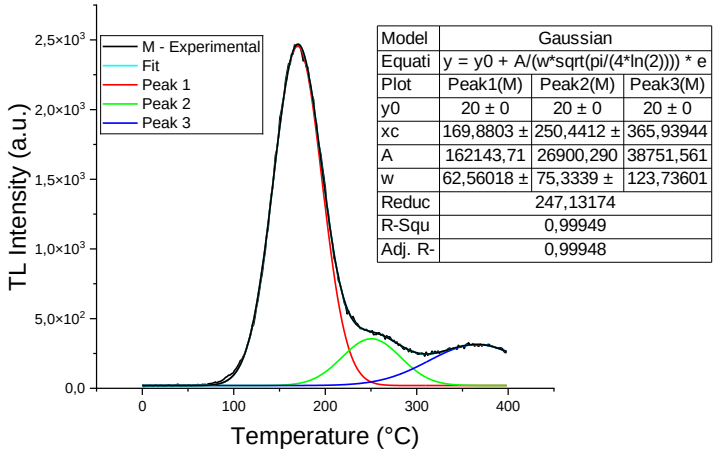
Model	Gaussian		
Equat	y = y0 + A/(w*sqrt(pi/(4*ln(2))))		
Plot	Peak1(A)	Peak2(A)	Peak3(A)
y0	20 ± 0	20 ± 0	20 ± 0
xc	158,3053	186,4923	344,8627
A	136866,9	49166,47	35978,54
w	45,51344	130,7353	86,89234
Redu	389,00101		
R-Squ	0,99942		
Adj. R	0,9994		

Figure 2: Deconvolution of the TL glow curves of sample T irradiated with 5 kGy.



Model	Gaussian		
Equati	y = y0 + A/(w*sqrt(pi/(4*ln(2)))) * exp(		
Plot	Peak1(C)	Peak2(C)	Peak3(C)
y0	19,1165 ±	19,1165 ± 0	19,1165 ± 0
xc	172,96782	191,50677	360,05715
A	171944,37 08 ± 3710,	73882,757 75 ± 3406,6	56576,056 86 ± 1266,5
w	54,33479 ±	96,34914 ±	123,61687
Reduc ed Chi-	345,90224		
R-Squ	0,99967		
Adj. R-	0,99966		

Figure 3: Deconvolution of the TL glow curves of sample T irradiated with 5 kGy.



Model	Gaussian		
Equati	y = y0 + A/(w*sqrt(pi/(4*ln(2)))) * e		
Plot	Peak1(M)	Peak2(M)	Peak3(M)
y0	20 ± 0	20 ± 0	20 ± 0
xc	169,8803 ±	250,4412 ±	365,93944
A	162143,71	26900,290	38751,561
w	62,56018 ±	75,3339 ±	123,73601
Reduc	247,13174		
R-Squ	0,99949		
Adj. R-	0,99948		

Figure 4: Deconvolution of the TL glow curves of sample M irradiated with 5 kGy.

3.3 EPR signal of unirradiated samples.

Figure 5 presents the EPR spectra of the unirradiated samples T, A, and M, recorded to characterize intrinsic paramagnetic centers and establish baseline signal intensities prior to irradiation. Since cowrie shells consist essentially of calcium carbonate ($CaCO_3$), the experimental parameters were based on literature references. The spectra are expected to reveal signals near $g \approx 2.0$, characteristic of the CO_2^- radical — the dominant species in biogenic aragonites under the studied conditions — alongside possible contributions from CO_3^- and NO_2^- impurities [10,11]. The presence of Mn^{2+} ions is also anticipated, as these are commonly found in $CaCO_3$-based biomaterials and produce a characteristic six-line hyperfine pattern near $g \approx 2.0$.

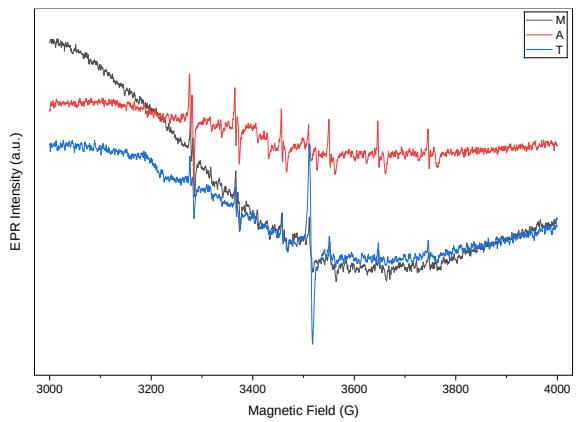


Figure 5: EPR signal intensity of the unirradiated samples T, A and M.

4. Conclusions

The signals observed through the EPR technique can be attributed to structural defects in the crystalline lattice of calcium carbonate, potentially induced by ionizing radiation. These defects give rise to paramagnetic centers, whereby the intensity of the obtained signal is proportional to the dose absorbed by the material, the fundamental basis for the high-dose dosimetric application of this material.

Acknowledgements

The authors acknowledge the partial financial support of the IPEN/CNEN (SEI: 01342.000256/2026-56).

References

[1] E. Yiridoe, "Economic and sociocultural aspects of cowrie currency of the Dagaaba of Northwestern Ghana.", *Nordic Journal of African Studies*, vol. 4, no. 2, pp. 16-16. (1995).
[2] B. Odunbaku, "Importance of cowrie shells in pre-colonial Yoruba land South Western Nigeria: Orile-Keesi as a case study," *International Journal of Humanities and Social Sciences*, vol. 2, no. 18, pp. 234–241 (2012).
[3] I. Ekin and R. Sesen, "Molluscs: their usage as nutrition, medicine, aphrodisiac, cosmetic, jewelry, cowrie, pearl, accessory and so on from the history to today," *Middle East Journal of Science*, vol. 4, no. 1, pp. 45–51 (2018).
[4] F. O. Ogundare, M. L. Chithambo, and B. O. Akintunde, "Optically stimulated luminescence of cowrie shells," *Applied Radiation and Isotopes*, vol. 167, p. 109463 (2021).
[5] M. Ikeya, "Radiation effects in organics and inorganics for ESR dosimetry," *Applied Radiation and Isotopes*, vol. 47, no. 11–12, pp. 1479–1481 (1996).
[6] M. Desrosiers and D. A. Schauer, "Electron paramagnetic resonance (EPR) biodosimetry," *Nuclear Instruments and Methods in Physics Research Section B: Beam Interactions with Materials and Atoms*, vol. 184, pp. 1–2 (2001).
[7] O. Duliu, "Comparative study on ESR spectra of carbonates," *nipne.ro* (2007).
[8] R. A. Vazirov, S. Y. Sokovnin, E. N. Agdantseva, A. N. Tsmokalyuk, and M. E. Balezin, "EPR measurement of radiation-treated chicken eggs," *AIP Conference Proceedings*, vol. 2174, p. 020186 (2019).
[9] E. Aboelezz and M. A. Sharaf, "Ostrich egg shell as an accurate retrospective dosimeter using electron paramagnetic resonance technique," *Scientific Reports*, vol. 16, p. 12148 (2026).
[10] J. Sadło, A. Bugaj, G. Strzelczak, M. Sterniczuk, and Z. Jaegermann, "Multifrequency EPR study on radiation induced centers in calcium carbonates labeled with ^{13}C," *Nukleonika*, vol. 60, pp. 429–434 (2015).
[11] A. Zarins, A. Antuzevics, G. Kizane, J. Leys, and R. Knitter, "Simulations of complex electron paramagnetic resonance spectra for radiation-induced defect centres in advanced ceramic breeder pebbles," *Nuclear Materials and Energy* (2023).